The influence of MHD boundary layers on tritium permeation in PbLi flows for fusion breeding blankets

F. R. Urgorri[a], C. Moreno[a], I. Fernández-Berceruelo[a], D. Rapisarda[a]

[a] *CIEMAT-LNF, Av. Complutense 40, Madrid 28040, Spain*

Abstract

In PbLi based breeding blanket concepts, tritium is produced inside the liquid metal and drag out of the reactor by the liquid metal flow. However, undesired permeation through the channels and pipes walls occurs spontaneously since tritium naturally diffuses in the opposite direction of the concentration gradient. This way tritium can reach the blanket coolant circuit or even the exterior with an impact on the tritium self-sustainability and the safety of the plant. Similarly to heat transfer processes, permeation through the walls in the interface between the flow and the steel is mostly affected by the dynamics of the boundary layers. This is ruled by the electrical coupling between the moving conductor and the conducting walls as a result of the Magnetohydrodynamics (MHD) interactions which dominate the flow dynamics. In this work, the connection between the MHD forces and tritium transport is numerically studied using the simulation platform ANSYS-Fluent. The velocity profiles of a PbLi test channel have been firstly computed in a wide range of Hartmann numbers from 10^2 to 10^4. These velocity profiles are then applied to a 3D tritium transport model developed with the customization capabilities of the same platform. A series of tritium transport simulations are carried out considering different permeation regimes: surface-limited, diffusion-limited and intermediate regimes. The development of the concentration boundary layers along the channel is studied in different permeation regimes, magnetic fields and velocity fields. This has allowed correlating the Sherwood number (*Sh*) with the Hartmann (*Ha*), Reynolds (*Re*) and permeation numbers (W).

Keywords: Mass transfer, Tritium transport, Magnetohydrodynamics, Breeding blanket

1. Introduction

Future fusion reactors by magnetic confinement will include a breeding blanket system able to, among other functions, regenerate the tritium burnt in the plasma. The tritium generated in this system has to be dragged out of the reactor for being processed, stored and eventually reinjected in the plasma. This way, the blanket and the rest of the systems associated to the tritium fuel cycle have to be designed to accomplish the so called tritium self-sustainability of the plant. Tritium permeation from the breeder to the blanket coolant loop or to the environment can threaten this function. Moreover, since tritium is a radioactive element, these losses can compromise the safety of the installation.

Some of the most promising breeding blanket concepts are based on a liquid alloy of Pb and Li that acts as the breeder, the neutron multiplier, the tritium carrier and provides shielding. This is the case of three of the concepts developed within the framework of EUROfusion [1] in the last years: the Helium Cooled Lithium Lead (HCLL) [2], the Dual Coolant Lithium Lead (DCLL) [3] and the Water Cooled Lithium Lead (WCLL) [4]. The later has been selected also for the Test Blankets Modules (TBM) program of ITER [5]. Therefore, a good understanding of the tritium transport phenomena from the PbLi to the solid materials is crucial for obtaining accurate predictions of the tritium behavior.

Tritium transport models aims at estimating the tritium permeation rates and inventories in the different locations of the blanket and the rest the associated systems. In particular, system level models allow computing the global tritium dynamics and they are important tools to evaluate the performance of any blanket concept and design [6, 7]. However, system level models describe very big systems which means that they have to introduce several assumptions and simplifications. These can lead to important uncertainties in the

Email address: fernando.roca@ciemat.es (F. R. Urgorri)

results as it has been observed in the sensitivity analyses performed with these models [8, 9].

Some of the uncertainties come from the experimental dispersion of a specific material property (e.g. the tritium solubility in Pbli [10]), others come from the lack of technological developments and prototypes of some parts of the system (e.g. the tritium extraction techniques [11, 12]). There is also an important uncertainty related to the simplifications of the multi-physical phenomena involved in the transport processes. This is the case of the tritium permeation through the MHD boundary layers (BLs) in liquid metal channels which is a process that is neglected on most system level analyses.

The mass and heat transfer phenomena through the BL have been studied in the past in hydrodynamic conditions (e.g. [13, 14]). Nevertheless, in breeding blanket applications the liquid metal dynamics is dominated by the MHD forces. These modify both the thickness and the shape of the velocity BLs and will have unavoidably an important impact on tritium permeation through the channel walls. Indeed, the effect of the magnetic field has been already observed in heat transfer experiments an analyses at relatively low intensities [15, 16].

Some of the past tritium transport models at system level included the effect of diffusive BLs with similar thickness than the MHD velocity layers [8]. This first approach most likely underestimates the permeation rate since the mass BLs are expected to be significantly thinner than the MHD ones. There are correlations for estimating the mass transfer coefficient that have been successfully applied to transport models in subsystems out of the blanket [17]. However, these correlations are not expected to be valid once the fluid dynamics is altered by the magnetic field.

In this paper, a comprehensive numerical study of the mass transport phenomena through pure MHD BLs in a test square-section channel is presented. The channel is immersed in a constant magnetic field transversal to the flow. A constant tritium concentration is imposed at the inlet of the channel while perfect vacuum conditions are applied to the external side of the channel walls (figure 1). Part of the incoming tritium will permeate through the channel walls while the rest leaves the system through the channel outlet.

Both MHD simulations and mass transfer simulations have been conducted with the finite volume method software ANSYS-Fluent. A total of 161 simulations have been carried out to cover wide ranges of the Hartmann number (Ha), the Reynolds number (Re) and the permeation number (W). The thickness and shape of the mass BLs are analyzed and the averaged Sherwood number (Sh) is obtained for each combination of parameters.

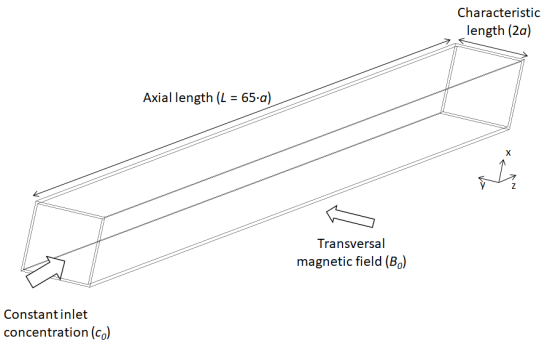

Figure 1: Test channel used for analyze the mass transfer phenomena

2. MHD computations

From the MHD point of view, the problem is treated using a fully developed flow approximation. This kind of MHD fully developed models have been used in fusion applications [18, 19]. Since the MHD forces strongly suppress the inertial effects and buoyancy forces, this approximation is expected to be valid in some straight channels of the breeding blanket. Indeed, the MHD flows remain laminar even at the high Reynolds numbers that can be found in the blanket channels. This laminarization is observed when $Re \lesssim 250Ha$ [20]. The square of the Hartmann number (Ha) represents the ratio between Lorentz and viscous forces:

$$Ha := aB_0 \sqrt{\frac{\sigma}{\eta}} \tag{1}$$

Where a is the characteristic length of the problem, B_0 is the applied magnetic field, σ is the conductivity of PbLi and η its dynamic viscosity.

The fully developed approximation reduces the original system of 6 equations and 6 variables (the three components of the velocity field and the three components of the induction magnetic field) to a system of 2 equations and 2 variables:

$$\eta\left(\partial_{xx}u + \partial_{yy}u\right) - \partial_z p + \frac{B_0}{\mu}\partial_y B_i = 0 \tag{2}$$

$$\mu^{-1}\left(\partial_x\left(\sigma^{-1}\partial_x B_i\right) + \partial_y\left(\sigma^{-1}\partial_y B_i\right)\right) + B_0\partial_y u = 0 \tag{3}$$

The computational problem is written in terms of the axial velocity (u) and the induced magnetic field (B_i)

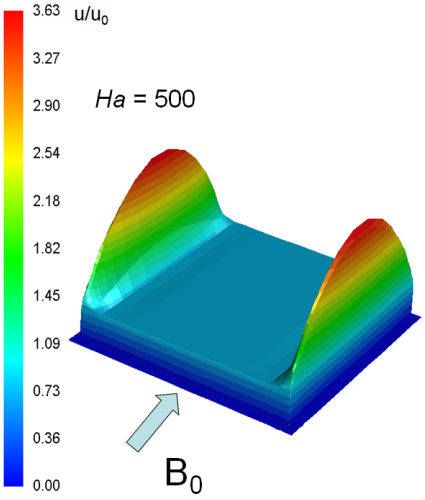

Figure 2: Fully developed MHD velocity profile in a square section channel with conductive walls

which lays parallel to the flow (z coordinate). In fully developed flows, the pressure gradient ($\partial_z p$) is constant.

The system of equations (2)-(3) has been solved numerically using the platform ANSYS-Fluent. A verification exercise of this kind of fully developed models in Fluent has been carried out using Shercliff and Hunt analytical solutions [19]. Besides, there have been validations works of the MHD Fluent solver against experiments [21] and a successful benchmarking activity against another 4 codes [22].

The numerical solution for the fully developed MHD flow with conductive walls is well known. The Lorentz forces produce a flat core flow while two different kinds of BLs are developed (figure 2). On the one hand, the so called Hartmann BLs have a similar shape than the hydrodynamic layers but much thinner. On the other hand, thin high velocity jets are developed in the so called side BL. The thickness of the BLs and the intensity of the jet depend on value of Ha. The Hartmann BL thickness is of the order of a/Ha while the side BL thickness is of the order of $a/\sqrt{Ha}$. The computed MHD BLs are exposed in figure 3 and figure 4 for different values of Ha. The flow is presented normalized by the average velocity u_0.

The intensity of the side jets depends not only on Ha but also on the product on the wall thickness (t_w) and the wall conductivity (σ_w). More precisely, this influence is determined by the wall conductivity ratio ($C_w = \sigma_w t_w / \sigma a$) which is typically of the order of 10^{-2} taking into account the conductivities of PbLi [23] and the wall steel.

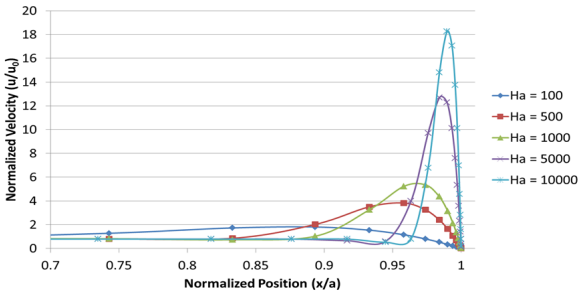

Figure 3: Normalized velocity profile at the side BL for different Ha

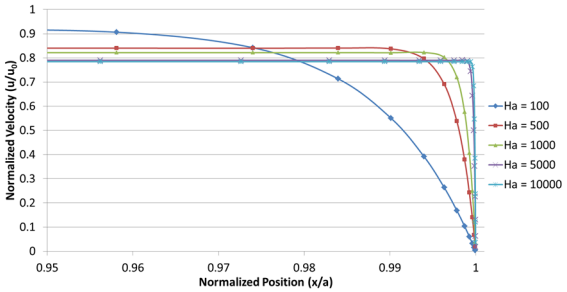

Figure 4: Normalized velocity profiles at the Hartmann BL for different Ha

Since the shape and the thickness of both kinds of layers are very different between each other, it is expected that the mass transfer through the Hartmann walls and the side walls would be different as well (even when the wall surfaces and thicknesses are the same). As a consequence, tritium permeation through the Hartmann and Side layers has to be analyzed independently. This means that two different mass transfer coefficients (and Sherwood numbers) are defined for this problem: one for the Hartmann layers and one for the side layers.

3. Mass transfer model

The fully developed MHD velocity profiles ($u(x, y, z)$) are used as an input for mass transfer simulations. The tritium transport problem is described by the mass continuity equation:

$$\partial_t c + \partial_i (u^i c - D\partial^i c) = S \tag{4}$$

Where $c(x, y)$ is the tritium concentration field, D is the diffusivity constant of the medium and S are the possible sink and sources. In the test channel analyzed, no volumetric sources or sinks have been considered

($S = 0$). The steady state is reached when the temporal term of the equation banishes.

Equation (4) is valid in both the solid and fluid domains. In the former one, the advection term is zero ($u = 0$). Differently from the heat transfer problems, the concentration field is not a continuous function across the interface fluid/solid. In agreement with Sieverts' law, there is a discontinuity in the concentration field that is given by the tritium solubility (K_s) at both sides of the interface:

$$\left(\frac{c_w}{K_s}\right)_{solid} = \left(\frac{c_w}{K_s}\right)_{fluid} \tag{5}$$

$$-D_{solid}\partial_n c_w = -D_{fluid}\partial_n c_w \tag{6}$$

Where c_w refers to the value of the concentration field at the internal side of the wall. The discontinuity (5) is a consequence of the equalization of the partial pressure at both sides of the interface. The tritium flux ($J_i = -D\partial_i c$) is logically continuous across the interface which ensures mass conservation. The concentration discontinuity can be treated numerically imposing internal boundary conditions. This can be done in Fluent using the so called User Defined Functions (UDFs) in a similar manner that was performed in [24]. However, in this work an alternative approach has been employed based in the following change of variable:

$$\psi := \begin{cases} \dfrac{c}{K_{sw}^{solid}} & x_i \in solid \\ \dfrac{c}{K_{sw}^{fluid}} & x_i \in fluid \end{cases} \tag{7}$$

Where K_{sw}^{solid} and K_{sw}^{fluid} are the solubility at the solid-fluid interface evaluated at the solid and fluid sides, respectively. Therefore, the new scalar field (ψ) is defined differently when it is evaluated in the solid or fluid domains. It has units of $Pa^{0.5}$ and it is continuous across the interface fluid-solid by definition. The tritium flux can be written in terms of the new scalar as follows:

$$J_i = -D\partial_i(K_{sw}\psi) = -D(K_{sw}\partial_i\psi + \psi\partial_i K_{sw}) \tag{8}$$

The change of variables is useful when $\psi\partial_i K_{sw} \ll K_{sw}\partial_i\psi$. This is verified when the wall solubility changes little, both in the solid and fluid sides. In the channel studied in this work this condition is fulfilled since constant average properties have been assumed ($\partial_i K_{sw} = 0$).

In this circumstances, the flux of the new scalar can be defined as a continuous function across the wall interface whose diffusivity is defined as: $\Phi = K_{sw} \cdot D$. The property Φ can be identified with the material permeability.

$$\psi_w\,|_{solid} = \psi_w\,|_{fluid} \tag{9}$$

$$-D \cdot K_{sw}\partial_n\psi_w\,|_{solid} = -D \cdot K_{sw}\partial_n\psi_w\,|_{fluid} \tag{10}$$

Finally, the evolution equation of the scalar field in the steady state can be derived from the continuity equation:

$$\partial_i(K_{sw} \cdot u^i\psi - K_{sw} \cdot D\partial^i\psi) = 0 \tag{11}$$

This equation is solved for the steady-state situation using the customization capabilities of Fluent. It is possible to define what it is called a User Defined Scalar (UDS) which evolves following a generic convection-diffusion equation [25]. The different terms of the equations can be defined as desired. In this case, the diffusivity term is given by $D \cdot K_{sw}$ while the convection term is given by the field $K_{sw} \cdot u_i$.

This way the problem can be solved without introducing internal boundary conditions. The change of variables (7) is reverted at the end of the simulation.

The final piece of the model is the boundary condition at the external side of the channel wall (J_e). In this kind of interface, dissociation and recombination processes of molecules take place [26]:

$$J_e = 2(\sigma k_1 p_{T2} - \sigma k_2 c_e^2) \tag{12}$$

Where k_1 and k_2 are the dissociation and recombination constants of the wall material, σ is the sticking coefficient of the surface, p_{T2} is the partial pressure of molecules outside the channel and c_e is the concentration at the external side of the wall. The factor 2 is present because for each T_2 molecule that dissociates of recombines, 2 tritium atoms enter or leave the solid.

In the present analyses it is assumed that the dissociation flux is negligible in comparison with the recombination flux. This represents for example, a situation in which there is a very big volume at the other side of the channel. This can represent also a situation in which an external flow (typically the coolant) removes the permeated tritium rapidly. In both cases, the partial pressure of molecules is expected to be close to zero.

After the change of variables, the recombination boundary condition for the scalar field ψ depends on the dissociation constant ($K_s^2 := k_1/k_2$):

$$J_e = -2\sigma k_2 K_s^2 \psi_e^2 = -2\sigma k_1 \psi_e^2 \tag{13}$$

Condition (13) is included in the Fluent model using a dedicated UDF. A verification exercise of the implementation of the recombination boundary condition can be found in [27].

A scheme of the mathematical model solved in this work in the fluid and solid domains is exposed in figure 5.

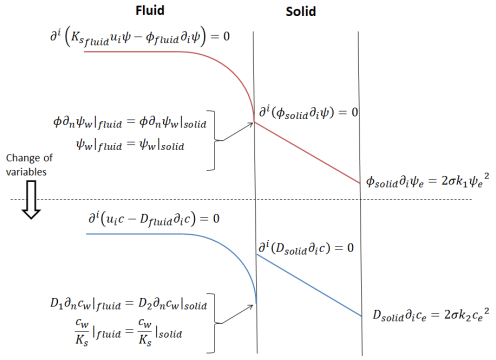

Figure 5: Scheme of the mathematical model solved for the scalar field ψ with a sketch of the solution for the ψ field (red curve) and tritium concentration field (blue curve)

4. Mass boundary layers

The velocity BLs produce variation in the advective term of the mass continuity equation ($u^i \partial_i c$) which are responsible of the mass BLs formation. When performing 1D transport analyses, it is useful to simplify the transport through the BL by linearizing the flux normal to the wall [17]:

$$J = K_t(c_0 - c_w) \tag{14}$$

The flux depends only on the difference between the concentration at the core (c_0) of the flow and the concentration at the interface with the wall (c_w). The proportionality constant is called the mass transfer coefficient. If the mass transport in the system is dominated by diffusion the mass transport coefficient tends to the diffusivity over the characteristic length ($K_t \to D/a$). If the advection effects are not negligible, the mass transfer coefficient is higher. The ratio between the advective mass transfer and diffusion mass transfer is given by the Sherwood number (Sh):

$$Sh := \frac{K_t \cdot a}{D} \tag{15}$$

The total permeation phenomenon is not only affected by the transport in the liquid metal but also by the permeation through the solid walls. This is heavily affected by the permeation regime of the system. This regime is determined by the relative weight of the surface phenomena with respect to the diffusion through the solid bulk.

The steady state flux through a rectangular membrane, with thickness t, constant concentration c at one side of it and recombination boundary condition at the other (equation (13) with $p = 0$), can be written as follows [27]:

$$J = D\frac{c}{t}\left[1 + \frac{1 - \sqrt{1 + 8W}}{4W}\right] \tag{16}$$

$$W = \frac{\sigma k_2 c t}{D} \tag{17}$$

W is a dimensionless number that has the same conceptual meaning than the permeation number originally defined for membranes between two gases [28]. When $W \ll 1$ the surface processes are much slower than the diffusion through the membrane and the system is in surface-limited regime. In the other limiting case, when $W \gg 1$ the diffusion processes are much slower than the surface ones which can be assumed as instantaneous (diffusion-limited regime). Only in the later limiting case, the mass transport phenomenon is analogous to heat transfer.

In the channel studied in this work, it is of interest to relate the permeation regime of the channel wall with the concentration scale in the PbLi. For this reason, the ratio between the fluid and solid solubilities has been introduced in the definition of the permeation number. The core concentration has been taken as the concentration scale in the PbLi instead of the interface concentration since it is the variable that could normally be measured and controlled.

$$W := \frac{\sigma k_2 c_0 t_w}{D} \frac{K_{s\,solid}}{K_{s\,fluid}} \tag{18}$$

Since the velocity BL formation depends on the inertial, viscous and MHD effects, the Sherwood number must depend on the Reynolds and Hartmann numbers. Moreover, the permeation regime modifies the boundary condition in the external side of the wall. Therefore, Sh is expected to depend also on W.

It is worth noting that the mass transfer coefficient and the boundary layer thickness are closely related. The higher the mass transfer coefficient is, the thinner the BL. Inside the channel the BL thickness would grow with the axial coordinate. Moreover, this thickness would also vary crosswise since the velocity profile also does. Therefore, both the BL thickness and the mass transfer coefficient present a spatial dependence ($K_t(x, y, z)$).

Due to this dependency, it is sometimes convenient to define average mass transfer coefficients at the surface of interest (Ω):

$$\langle K_t \rangle = \frac{\int_\Omega K_t ds}{\int_\Omega ds} = \frac{1}{A} \int_\Omega \frac{J_n}{c_0 - c_w} ds \tag{19}$$

Where A is the area of the surface. In this paper, average mass transfer coefficients have been computed using the numerical values of fluxes and concentrations in the interfaces PbLi/wall. These are used to compute $\langle Sh \rangle$ for each kind of interface and to find the dependency on Re, Ha and W. The first 5 characteristic lengths of the channel have not been included in the averaging in order to avoid edge effects.

Since the Hartmann and side BLs have different thicknesses and shapes, two kinds of Sherwood numbers have been defined in this system: The side Sherwood number denoted by $\langle Sh \rangle_{side}$ and the Hartmann one, denoted by $\langle Sh \rangle_{Ha}$.

5. Computational results

The analyses performed consider a broad range of Re, Ha and W numbers. These are selected to include relevant conditions for PbLi based breeding blanket applications: $Re \in [5 \cdot 10^2, 10^5]$, $Ha \in [10^2, 10^4]$ and $W \in [10^{-3}, 10^3]$.

The thickness of the BLs and their development from the inlet of the channel towards the outlet depends on the conditions imposed (Ha, Re and W). Quantitatively, the differences between the different cases can be notorious. However, the results are qualitatively similar. In every case, two different kinds of mass BLs are formed as a result of the differences between the velocity BLs: The side mass BLs and the Hartmann mass BLs.

Considering for example a scenario with $Re = 10^4$, $Ha = 10^3$ and $W = 10^3$ (diffusion-limited regime), figure 6 depicts the concentration field in the channel walls (liquid metal side). The shape of the concentration contours is different for the Hartmann and side walls. In

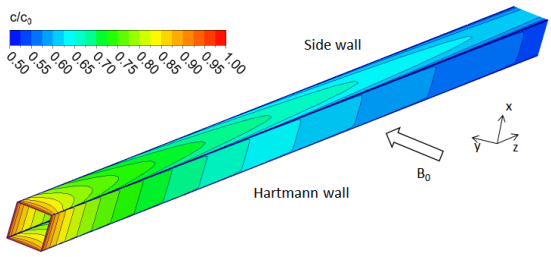

Figure 6: Concentration field in the wall of the channel (fluid side) for $Re = 10^4$, $Ha = 10^3$ and $W = 10^3$

both cases the concentration falls with the axial coordinate (z) but at a different rate. Moreover, the contours have a different dependence with the cross-sectional coordinates (x, y). On the one hand, the flat velocity profile next to the Hartmann layers, produces also a uniform concentration profile along the direction perpendicular to the magnetic field (x). On the other hand, at the side mass BLs the concentration exhibits a curvature along the direction parallel to the magnetic field (y). This is a consequence of the shape of the velocity jet at the side BLs (figure 2).

A clearer picture can be obtained when plotting the concentration along lines perpendicular to the channel walls and across the BLs. This view is exposed in figure 7 and figure 8 for a case with $Re = 10^3$, $Ha = 5 \cdot 10^3$ and $W = 1$ (intermediate permeation regime). The discontinuity in the concentration introduced by the solubility ratio can be clearly observed. In this work, this ratio is set to 1.217 which is the ratio between the tritium solubilities of EUROFER steel [29] and PbLi [30] at 350 ^{o}C.

In this paper, the thickness of the BLs (δ) have been defined as the thickness for which the concentration has dropped 10% of the concentration difference between the core concentration (c_0) and the concentration at the wall ($c_w = c(x = a)$):

$$[c(x = \delta) - c_w] = 0.9 \cdot [c_0 - c_w] \tag{20}$$

Figure 9 and figure 10 depict the shape of the boundary layers at three different axial locations. The BLs thickness present a decelerated growth along the flow direction. In the corners of the channels the shape of the two kinds of mass BLs are combined creating intermediate forms.

In this case, the layers are relatively thin, around 1% or 2% of the characteristic length of the problem. This would imply relatively high mass transfer coefficients (and Sh). For smaller Re, the BL thickness is close to

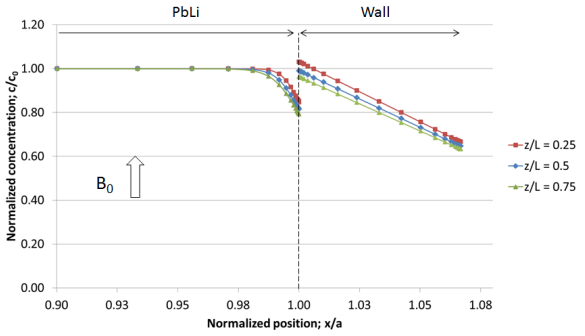

Figure 7: Concentration profile along a central line perpendicular to the side wall ($y = 0$) at different axial positions ($Re = 10^3$, $Ha = 5 \cdot 10^3$, $W = 1$)

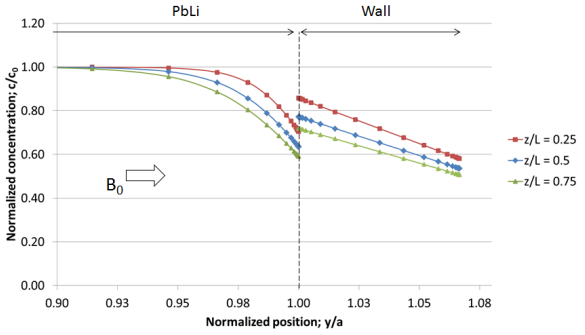

Figure 8: Concentration profile along a central line perpendicular to the Hartmann wall ($x = 0$) at different axial positions ($Re = 10^3$, $Ha = 5 \cdot 10^3$, $W = 1$)

the 8% of the characteristic length. Figure 11 expose the axial dependency of the BL thickness. In this case, the mass Hartmann BL is thicker than the side one but this is not true in every condition as it is shown in the following sections.

6. The effect of the Reynolds number

In this work, 5 different values of Re have been considered: $Re = 5 \cdot 10^2, 10^3, 5 \cdot 10^3, 10^4, 5 \cdot 10^4$ and 10^5. The high values of Re are characteristic of the feeding and collecting manifolds and pipes of fusion breeding blankets.

In the cases considered in the analyses, Re remains below the limit $Re < 250Ha$. For Re below the limit, the Hartmann boundary layers are expected to be fully laminarized [20]. However in some breeding blanket applications, a quasi-2-dimensional (Q2D) turbulence behavior can arise in the side BLs for Re values below the

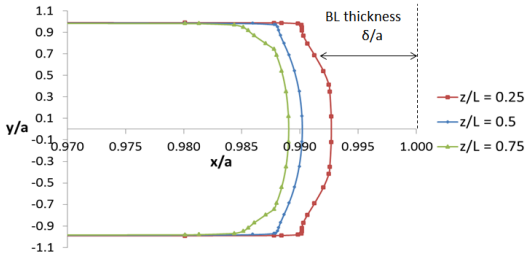

Figure 9: Cross-section shape of the mass side BLs at different axial positions for $Re = 10^4$ $Ha = 10^3$ and $W = 10^3$

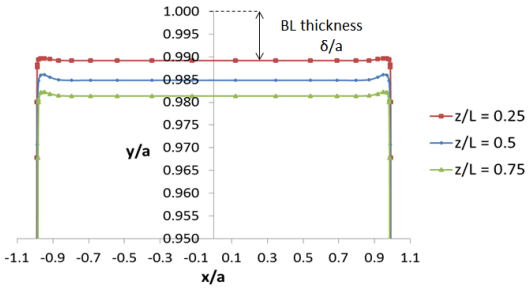

Figure 10: Cross-section shape of the mass Hartmann Bls at different axial positions for $Re = 10^4$ $Ha = 10^3$ and $W = 10^3$

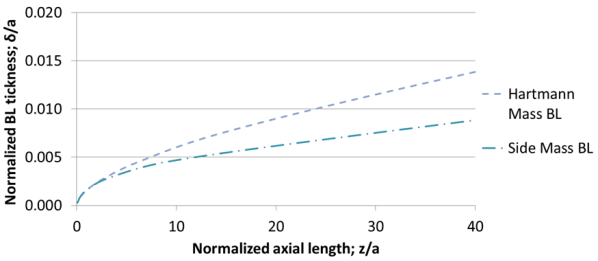

Figure 11: Mass BL thickness at the center of the Hartmann and side walls. ($Re = 10^4$, $Ha = 10^3$ and $W = 10^3$)

limit, specially when buoyancy effects are considered. This means that some cylindrical vortical structures can appear aligned with the magnetic field close to the side BLs. The magnetic field tends to suppress those structures quite effectively as well [31] but their appearance depends also on the strength of the buoyancy interaction (Grashof number).

The effect of Q2D turbulence and other instabilities in the side layers cannot be reproduced with a fully developed velocity profile and their influence on mass transfer is not included in the present analyses. The instabilities and Q2D vortexes are expected to increase the mass transfer in comparison with the fully laminarized solution.

The effect of changing Re is different for the side and

Hartmann BLs. This can be observed in figure 12 and figure 13. These depict the development of the BLs along two curves placed at the central part of the side wall ($y = 0$) and at the central part of the Hartmann wall ($x = 0$), respectively. Results correspond to a diffusion-limited regime situation ($W = 10^3$).

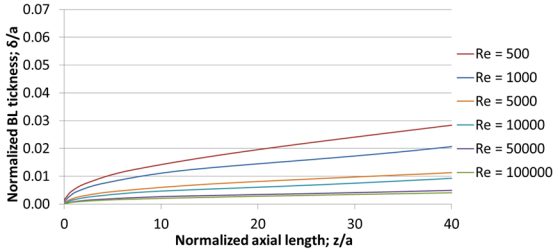

Figure 12: Central side mass BL for $Ha = W = 10^3$

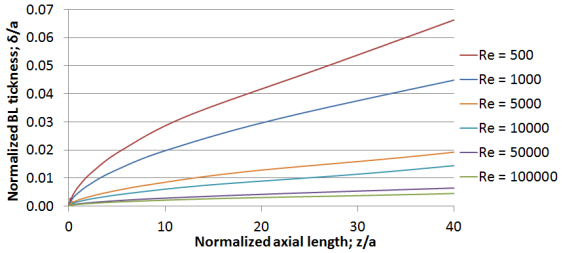

Figure 13: Central Hartmann mass BL for $Ha = W = 10^3$

As expected, the higher the Re is the thinner the Bls are. In this scenario, the Hartmann BLs grow in thickness faster than the side BLs. This means that the permeation through the side BLs is higher than through the Hartmann layer. However, this statement cannot be generalized for every conditions. For example, the difference between both kinds of layers mitigates at high Re where both become quite thin and comparable (specially for moderate Ha).

The effect of the Re cannot be separated easily from the effect of the magnetic field. This coupling is a consequence of the shape of the MHD profiles which creates BLs very different from the hydrodynamic ones. Figure 14 depicts $\langle Sh \rangle$ computed for the Hartmann and side BLs at different Ha and Re in surface-limited regime ($W = 10^{-3}$).

In general, both the Ha and the Re enhance mass transfer through the BLs since they strengthen the effect of advection. Due to the formation of the high velocity jets (figure 3), the mass transfer through side BLs is boosted by the increase of the magnetic field. In contrast, an increase of Re has a comparable effect on the permeation through the Hartmann and side BLs. These qualitative statements are found valid for every permeation regime.

For all values of Ha and W considered in this work, the same kind of dependence of $\langle Sh \rangle$ on Re is obtained. The usual power function fits accurately the results of simulations. However, the parameters of the fittings depend importantly on the specific Ha and W considered. Therefore, it is possible to write the first piece of a complete correlation as follows:

$$\langle Sh \rangle_{Ha/side} \simeq Sh_0(Ha, W) \cdot Re^{\alpha(Ha,W)} \tag{21}$$

Naturally, the functions $Sh_0(Ha, W)$ and $\alpha(Ha, W)$ have two different versions, one for the Hartmann BLs and one for the side ones. The range of the obtained exponents are a consequence of the laminarization of the flow. Indeed, the exponents are contained in between $1/3$ and $1/2$ which are in agreement with classical correlations of heat transfer in laminar flows that predict an exponent of $1/3$ [32]. In fact, the simulation with the conditions closer to laminar heat transfer conditions ($Ha = 10^2$ and $W = 10^3$) presents exponents close to $1/3$: $\alpha_{Ha} \simeq 0.39, \alpha_{side} \simeq 0.36$. In every simulation, the results are far from the predictions of the correlations for turbulent flows which consider exponents between 0.8 and 0.95 [13, 33, 34].

7. The effect of the Hartmann number

In the previous section it is mentioned that an increase of the external magnetic field enhances the mass transfer phenomena. This is caused by two different effects. Firstly, the magnetic field drastically reduces the thickness of the velocity BLs. This introduces a reduction of the mass BLs thickness with the corresponding increase of the permeation rate. This effect is dominant in the Hartmann BLs and it is particularly notorious when going from small Ha to moderate Ha. However, since the thickness of the Hartmann BL scales with Ha^{-1}, it does not change significantly once Ha is high. This saturation can be well observed in figure 15: Increasing the magnetic field produces an increase of the permeation (represented by the concentration slope in the solid) but this effect saturates when reaching high Hartmann numbers ($Ha > 10^3$).

The second effect is caused by the velocity jet produced by the MHD interaction. Having high velocity regions located very close to the permeation surface boosts the mass transfer via advection. This effect is expected to be dominant at high Ha since the velocity

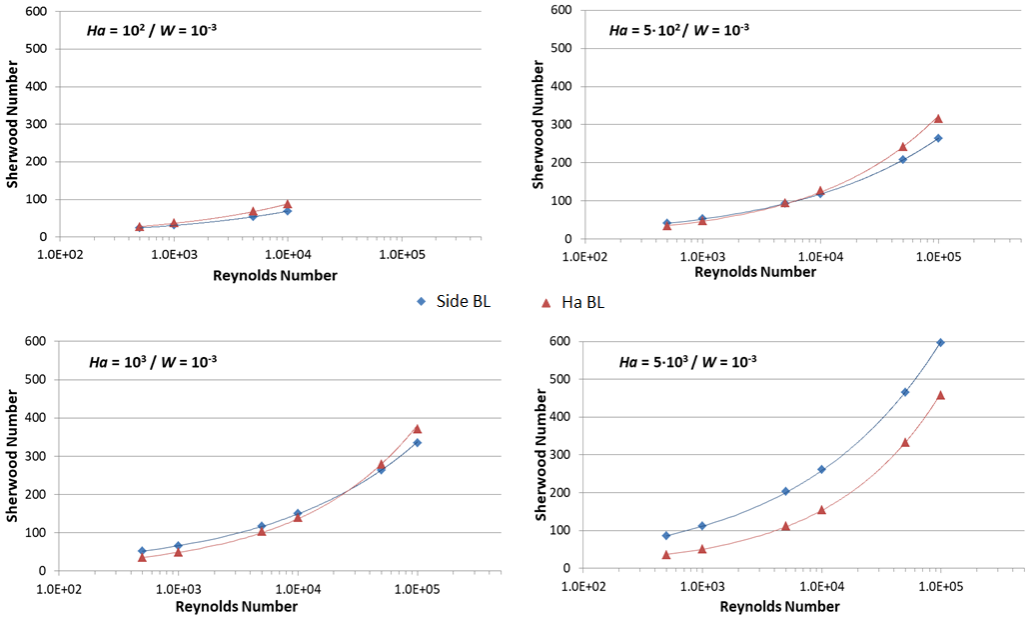

Figure 14: $\langle Sh \rangle$ as a function of Re for different Ha in surface-limited regime ($W = 10^{-3}$)

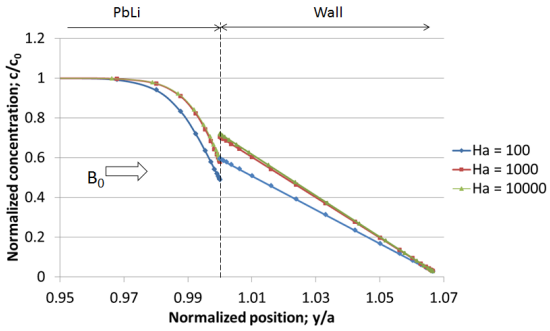

Figure 15: Concentration profile across a central line perpendicular to the Hartmann wall ($x = 0$) at the axial position $z/L = 0.75$ for different values of Ha. The conditions are $Re = 10^4$ and diffusion-limited regime ($W = 10^3$)

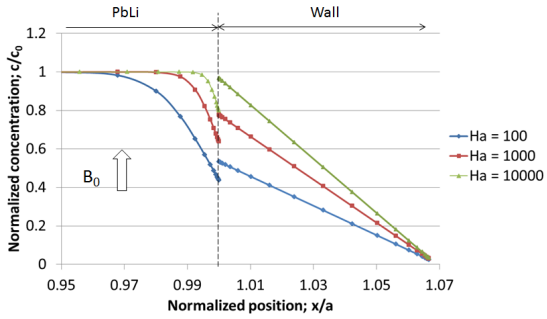

Figure 16: Concentration profile across a central line perpendicular to the side wall ($y = 0$) at the axial position $z/L = 0.75$ for different values of Ha. The conditions are $Re = 10^4$ and diffusion-limited regime ($W = 10^3$)

jets are more intense the higher Ha is (figure 3). Therefore, an advection dominant mass transfer (i.e. high Sh) through the side BLs is expected at high Ha. The enhancement of the permeation through the side BLs due to the magnetic field can be observed in figure 16.

The differences between both kind of BLs and the effects that dominates the permeation through them affect the mass BL thicknesses as exposed in figure 17 and figure 18. On the one hand, the thickness of the mass Hartmann BL scales with $\sim Ha^{-1}$ exactly as the velocity BL. On the other hand, the thickness of the mass side BL scales with $\sim Ha^{-0.14}$ which is different than the velocity one ($Ha^{-0.5}$). This difference is due to the velocity jet whose intensity increases the mass transfer through the side BL.

The saturation of the mass Hartmann layer thickness is also present in the dependence of $\langle Sh \rangle_{Ha}$ on Ha. Results in diffusion-limited regime ($W = 10^3$) are exposed in figure 19. This dependence is in qualitative agreement with previous heat transfer calculations of laminar flows in insulated pipes [35].

Complementary, figure 20 depicts the dependence of $\langle Sh \rangle_{side}$ on Ha. In this case, $\langle Sh \rangle$ increases faster but there is also a saturation effect at high Ha. This saturation is significantly slower than in the Hartmann BLs. As a consequence, the permeation rates are higher

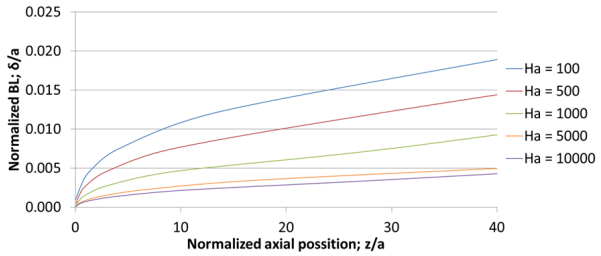

Figure 17: Side mass boundary layer thickness as function of the axial position in the central part of the wall ($y = 0$). The conditions are $Re = 10^4$ and diffusion-limited regime ($W = 10^3$)

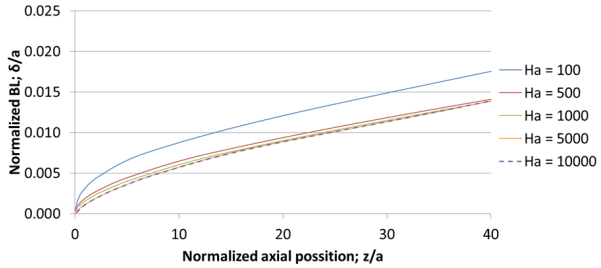

Figure 18: Harmnann mass boundary layer thickness as function of the axial position in the central part of the wall ($x = 0$). The conditions are $Re = 10^4$ and diffusion-limited regime ($W = 10^3$)

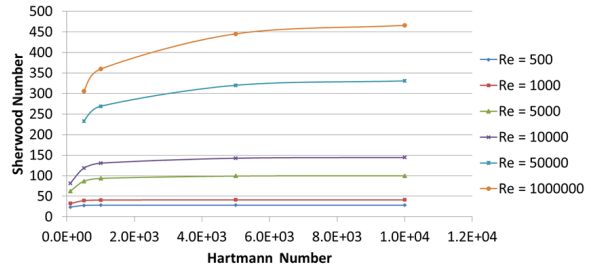

Figure 19: Average Sherwood number in the Hartmann BL for different Re as function of Ha ($W = 10^3$)

through the side BLs except when Ha is small.

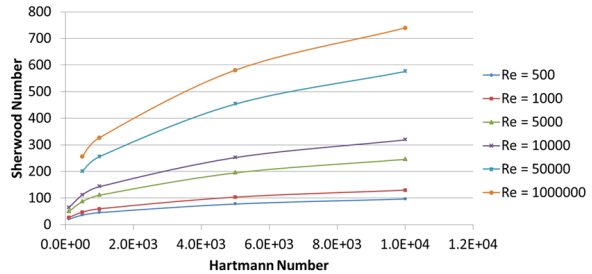

Figure 20: Average Sherwood number in the side BL for different Re as function of Ha ($W = 10^3$)

With the aim of finding a correlation for the Sherwood number ($\langle Sh \rangle = f(Re, Ha, W)$), the results of the simulations at different Ha have been used for finding a fitting for the functions $Sh_0(Ha, W)$ and $\alpha(Ha, W)$ present in equation (21). As obtained in [15] for heat transfer in pipes under magnetic field, it was found that rational expressions provide good fittings for both kind of functions:

$$Sh_0(Ha, W)_{Ha/side} \simeq \frac{K(W) + b(W) \cdot Ha}{1 + c \cdot Ha} \tag{22}$$

$$\alpha(Ha, W)_{Ha/side} \simeq \frac{\kappa(W) + \beta(W) \cdot Ha}{1 + \gamma \cdot Ha} \tag{23}$$

In the limiting case of $Ha \to 0$, the side and Hartmann BLs tend to regular hydrodynamic BLs. Therefore, the following constraint has to be maintained:

$$\langle Sh \rangle_{side}(Re, Ha = 0, W) = \\ = \langle Sh \rangle_{Ha}(Re, Ha = 0, W) \tag{24}$$

As a result, during the fitting process it has been imposed that: $K_{Ha} = K_{side}$ and $\kappa_{Ha} = \kappa_{side}$. Figure 21 and figure 22 depict the functions Sh_0 and α in surface and diffusion-limited regimes, respectively. The symbols represent the numerical data while the solid lines represent the rational function (22) and (23). The domain has been extended far from the numerical cases to observe the limit cases when $Ha \to 0$ and when $Ha \to \infty$.

The coefficients of the rational functions (22) and (23) depend on the permeation number W. The strongest dependence is found to be in $K(W)$. However, a weaker dependence is also found in the coefficients: κ, b and β. The variations in the denominator coefficients: c and γ with W are found to be small. Therefore, the same values are proposed for every permeation regime. These are exposed in table 1.

Table 1: Constant parameters of the functions (22) and (23)

	Hartmann BL	Side BL
c	$1.24 \cdot 10^{-3}$	$3.49 \cdot 10^{-4}$
γ	$2.04 \cdot 10^{-3}$	$4.68 \cdot 10^{-4}$

8. The effect of the permeation number

The permeation phenomenon across the channel walls is determined by the permeation regime. In this

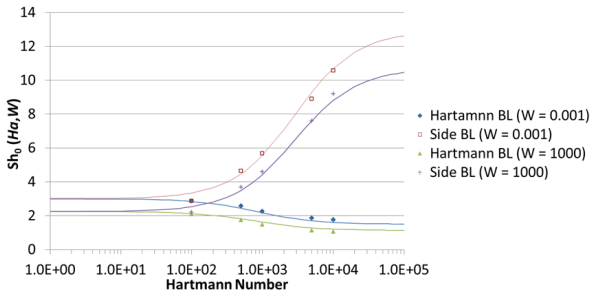

Figure 21: Sh_0 (21) as a function of Ha for surface-limited ($W = 10^{-3}$) and diffusion-limited regime ($W = 10^3$). Symbols represent the numerical results while solid lines corresponds to the rational fittings found

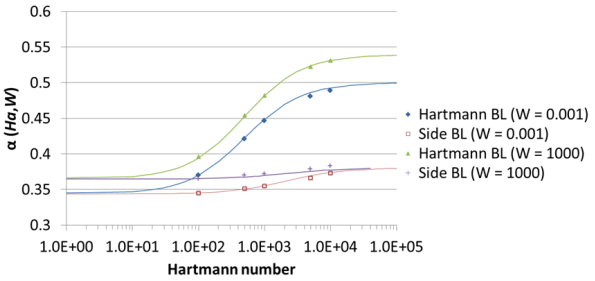

Figure 22: α (21) as a function of Ha for surface-limited ($W = 10^{-3}$) and diffusion-limited regime ($W = 10^3$). Symbols represent the numerical results while solid lines corresponds to the rational fittings found

paper, 7 values of the permeation parameter have been considered: $W = 10^{-3}, 10^{-2}, 10^{-1}, 10^{0}, 10^{1}, 10^{2}$ and 10^3. Since the permeation through the wall and through the BLs are affected by the external boundary condition, it is expected that the permeation regime will have some influence on the mass BLs formation.

In figure 23 it can be noticed the influence of W not only on the concentration profile across the channel wall but also across the side BL. The closer the system is to the diffusion-limited scenario the highest the concentration drop ($c_0 - c_w$) in the BL is.

In relative terms, surface-limited scenarios present the highest permeation flux and they will also present the highest mass transfer coefficient through the BL. However, in order to reach surface-limited regimes the core concentration (c_0) is usually very small. As a consequence, the absolute fluxes are much higher in diffusion-limited scenarios than in surface-limited scenarios.

Despite the very significant influence that W has on the permeation flux, it is found that the influence on Sh is significantly less important than either Ha or Re. This

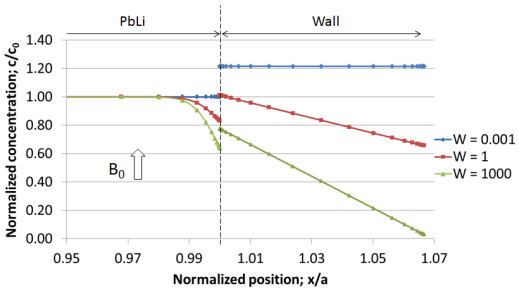

Figure 23: Concentration profile along a central line perpendicular to the side wall ($y = 0$) for different values of W ($Re = 10^4$ and $Ha = 10^3$)

means that the permeation regime mostly changes the concentration drop at the interface ($c_0 - c_w$) but the effect on the mass transfer coefficient is much more moderate.

Figure 24 depicts $\langle Sh \rangle$ as a function of W for two different values of Ha. In both cases, $\langle Sh \rangle$ presents a soft sigmoidal transition from the surface-limited to the diffusion-limited scenario. It can be observed how the effect of changing W is limited in comparison with the strong effect of Ha in both the Hartmann and side BLs.

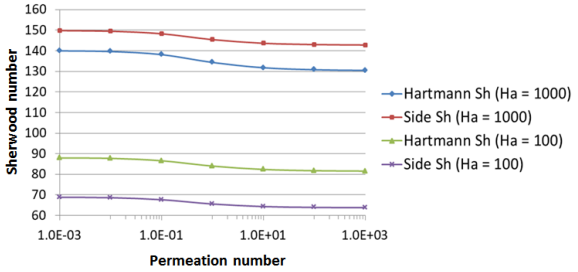

Figure 24: Sherwood number as a function of the permeation number for two different values of Ha and $Re = 10^4$

The final pieces of the correlation ($\langle Sh \rangle = f(Re, Ha, W)$), are the functions: K, κ, b and β. As mentioned in the previous section, the most important effect of W on the global correlation is located in the function $K(W)$. Observing the behavior of figure 24 sigmoidal functions have been tried for fitting the numerical results:

$$K(W) \simeq K_0 + \frac{\delta}{1 + \epsilon \cdot W^p} \tag{25}$$

The computational data fits very well the sigmoidal function as it can be observed in figure 25.

The same kind of functions have been used also for fitting κ, b and β. Only in the last case the sigmoidal fitting is not as good as in the others but the variations

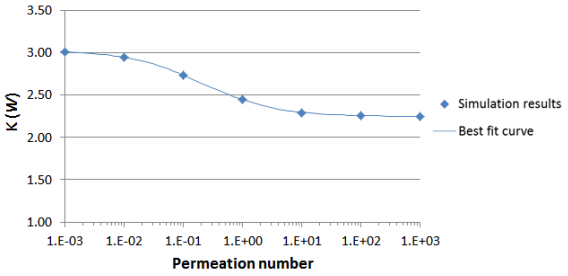

Figure 25: Function K present in (22) and (23)

of β with W are much smaller. In fact, in the case of the side layer, it is preferred to use a constant value instead of a sigmoidal function for β_{side}. The values of the coefficients coming from the fitting process are exposed in table 2.

Table 2: Constant parameters of the functions (22) and (23)

	K_0	δ	ϵ	p
K	2.24	0.78	2.98	0.69
κ	0.36	$-2.11 \cdot 10^{-2}$	4.79	0.84
b_{Ha}	$1.92 \cdot 10^{-3}$	$-5.20 \cdot 10^{-4}$	0.01	-0.95
b_{side}	$2.73 \cdot 10^{-3}$	$8.83 \cdot 10^{-4}$	2.73	0.98
β_{Ha}	$1.10 \cdot 10^{-3}$	$-8.50 \cdot 10^{-5}$	0.60	2.10
β_{side}	$1.78 \cdot 10^{-4}$	0	0	0

With these coefficients, the correlations for both the side and Hartmann BLs are complete. However, the derivation of a general correlation valid in the whole domain of Re, Ha and W involves relatively complex functions. During the fitting processes small deviations appear in some of the fitted functions at some parts of their domains. At the end of the whole process these errors sum up producing certain deviations between the Sherwood numbers obtained with the numerical data and those obtained with the correlations. Figure 26 depicts these deviations for different values of Re, Ha, W. The highest obtained deviation is approximately 16% which corresponds to the side BLs at low magnetic fields. In the best cases scenario, the matching is very good with deviation below 0.2%. In most of the cases, the deviation is contained between 1% and 10%.

9. Conclusions

This work is a comprehensive numerical investigation of the tritium permeation phenomenon through the MHD boundary layers of laminarized PbLi flows.

Fully developed MHD velocity profiles in conducting channels have been computed up to $Ha = 10^4$. The different velocity profiles obtained have been used for a series of steady state tritium transport computations. Both steps have been carried on using the simulation platform ANSYS-Fluent. The effect of changing the velocity field (Re), the magnetic field (Ha) and the inlet concentration field (W) has been studied.

The magnetic field is found to have a very significant influence on the developing of the mass BL. It has been confirmed that the permeation process behaves very differently across the two kind of MHD boundary layers: the Hartmann layers and the side layers. The former ones are only affected by the layer thickness while the later are also influenced by the presence of velocity jets. In general, the magnetic field importantly enhances the tritium permeation via the advection mechanism through the side BLs. However, it is important noting that, if a volumetric tritium generation source is considered inside the PbLi, the velocity jets will help removing the tritium generated inside the side layer. This effect should be studied in future developments.

Despite having a major impact on the permeation rate through the channel walls, the permeation number affects more weakly the mass transfer coefficients through the BL. This means that the permeation number affects tritium permeation rate primarily by changing the concentration difference between the core concentration (c_0) and the concentration at fluid-solid interface (c_w).

The averaged Sherwood number has been evaluated using the fluxes and concentrations computed at the channel walls interface. Except at very small Re and Ha, the mass transfer is dominated by the advection mechanism. Indeed, $\langle Sh \rangle$ can reach values of the order of 10^2. As a result, significantly thin boundary layers are developed in most of the studied cases.

A correlation between $\langle Sh \rangle$ and the other dimensionless numbers has been found. Similarly to past correlations derived for the Nusselt number, a power dependence on Re and a rational dependence on Ha have been found for the Sherwood number. In the case of the dependence on W, a soft sigmoidal transition from surface-limited regime to diffusion-limited regime has been obtained. For this last dependence, there is no heat transfer process analogous to surface recombination and dissociation of molecules.

The values Re, Ha and W considered in the analyses are relevant for PbLi based fusion breeding blanket applications. Nevertheless, breeding blankets are more complex systems that the test channel analyzed in this work. Real PbLi flows in breeding blankets can deviate from the fully developed approximation considered. In-

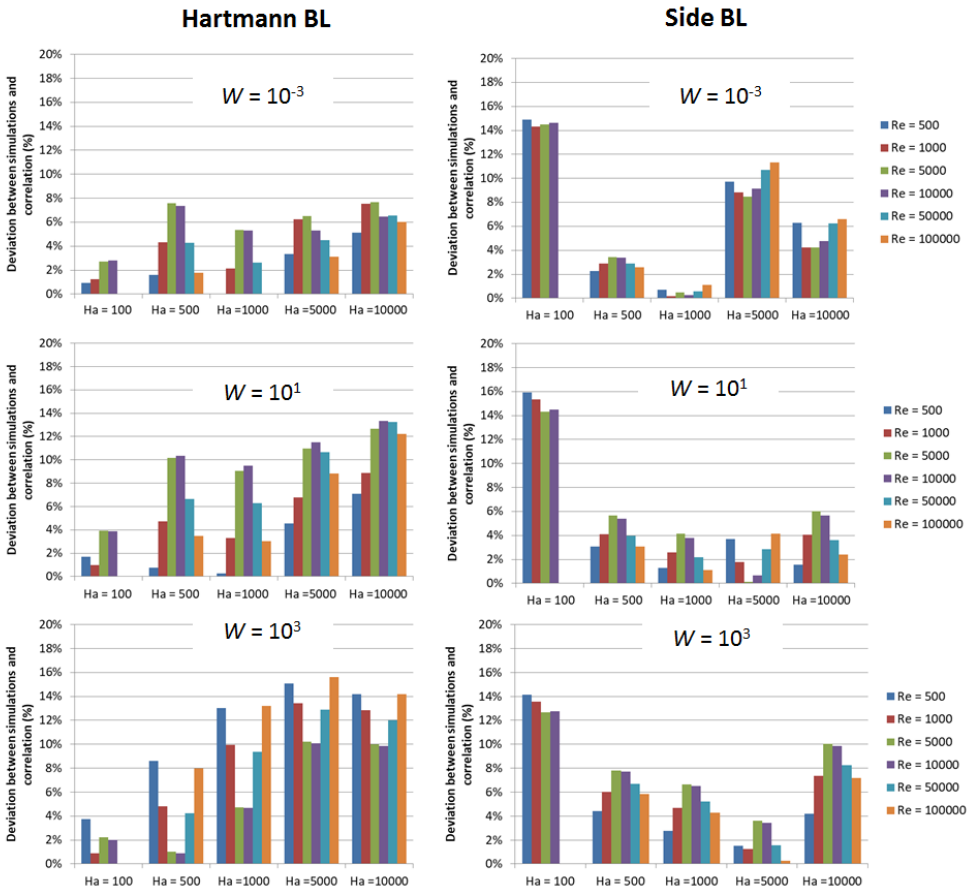

Figure 26: Deviation between the averaged Sherwood number computed with the numerical data and with the correlations

deed, mixed-convection effects, Q2D turbulence or inertial effects are expected to be present in some locations of the PbLi flow path, depending on the design specifics. Those effects are in principle expected to increase the mass transfer through the channel walls via advection. In addition, some blanket designs present electrical insulation components, such as flow channel inserts or ceramic coatings [36]. In principle, those components should reduce the permeation rate as the ceramics are typically good permeation barriers. All these effects should be added in future simulations in order to analyze their impact on tritium transfer.

Acknowledgments

This work has been carried out within the framework of the EUROfusion Consortium and has received funding from the Euratom research and training programme 2014-2018 and 2019-2020 under grant agreement No 633053. The views and opinions expressed herein do not necessarily reflect those of the European Commission.

This work was partially supported by the computing facilities of Extremadura Research Centre for Advanced Technologies (CETA-CIEMAT), funded by the European Regional Development Fund (ERDF). CETA-CIEMAT belongs to CIEMAT and the Government of Spain.

References

[1] L. Boccaccini, G. Aiello, J. Aubert, C. Bachmann, T. Barrett, A. Del Nevo, D. Demange, L. Forest, F. Hernandez, P. Norajitra, G. Porempovic, D. Rapisarda, P. Sardain, M. Utili, L. Vala, Objectives and status of EUROfusion DEMO blanket studies, Fusion Engineering and Design 109-111 (2016) 1199 – 1206. doi:https://doi.org/10.1016/j.fusengdes.2015.12.054.

[2] G. Aiello, J. Aubert, N. Jonqures, A. L. Puma, A. Morin, G. Rampal, Development of the helium cooled lithium lead blanket for DEMO, Fusion Engineering and Design 89 (7) (2014) 1444–1450. doi:https://doi.org/10.1016/j.fusengdes.2013.12.036.

[3] D. Rapisarda, I. Fernandez, I. Palermo, M. Gonzalez, C. Moreno, A. Ibarra, E. Mas de les Valls, Conceptual design of the EU-DEMO dual coolant lithium lead equatorial module, IEEE Transactions on Plasma Science 44 (9) (2016) 1603–1612.

[4] A. Del Nevo, P. Arena, G. Caruso, P. Chiovaro, P. Di Maio, M. Eboli, F. Edemetti, N. Forgione, R. Forte, A. Froio, F. Giannetti, G. Di Gironimo, K. Jiang, S. Liu, F. Moro, R. Mozzillo, L. Savoldi, A. Tarallo, M. Tarantino, A. Tassone, M. Utili, R. Villari, R. Zanino, E. Martelli, Recent progress in developing a feasible and integrated conceptual design of the WCLL BB in EUROfusion project, Fusion Engineering and Design 146 (2019) 1805 – 1809. doi:https://doi.org/10.1016/j.fusengdes.2019.03.040.

[5] J. Aubert, G. Aiello, D. Alonso, T. Batal, R. Boullon, S. Burles, B. Cantone, F. Cismondi, A. Del Nevo, L. Maqueda, A. Morin, E. Rodrguez, F. Rueda, M. Soldaini, J. Vallory, Design and preliminary analyses of the new water cooled lithium lead TBM for ITER, Fusion Engineering and Design 160 (2020) 111921. doi:https://doi.org/10.1016/j.fusengdes.2020.111921.

[6] P. W. Humrickhouse, B. J. Merrill, Tritium aspects of the fusion nuclear science facility, Fusion Engineering and Design 135 (2018) 302 – 313. doi:https://doi.org/10.1016/j.fusengdes.2017.04.099.

[7] E. Carella, C. Moreno, F. R. Urgorri, D. Rapisarda, A. Ibarra, Tritium modelling in HCPB breeder blanket at a system level, Fusion Engineering and Design 124 (2017) 687–691. doi:https://doi.org/10.1016/j.fusengdes.2017.01.051.

[8] F. R. Urgorri, C. Moreno, E. Carella, D. Rapisarda, I. Fernández-Berceruelo, I. Palermo, A. Ibarra, Tritium transport modeling at system level for the EUROfusion dual coolant lithium-lead breeding blanket, Nuclear Fusion 57 (11) (2017) 116045. doi:https://doi.org/10.1088/1741-4326/aa7f9d.

[9] A. Santucci, A. Ciampichetti, D. Demange, F. Franza, S. Tosti, Tritium migration in HCLL and WCLL blanket s: Impact of tritium solubility in liquid Pb-17Li, IEEE Trans. Plasma Sci. 42 (4) (2014) 1053–1057.

[10] S. Fukada, T. Terai, S. Konishi, K. Katayama, T. Chikada, Y. Edao, T. Muroga, M. Shimada, B. Merrill, D. K. Sze, Clarification of tritium behavior in PbLi blanket system, Materials Transactions 54 (4) (2013) 425–429. doi:https://doi.org/10.2320/matertrans.MG201203.

[11] B. Garcinuño, D. Rapisarda, R. Antunes, M. Utili, I. Fernández-Berceruelo, J. Sanz, Á. Ibarra, The tritium extraction and removal system for the DCLL-DEMO fusion reactor, Nuclear Fusion 58 (9) (2018) 095002. doi:https://doi.org/10.1088/1741-4326/aacb89.

[12] M. Utili, A. Aiello, L. Laffi, A. Malavasi, I. Ricapito, Investigation on efficiency of gas liquid contactor used as tritium extraction unit for HCLL-TBM Pb-16Li loop, Fusion Engineering and Design 109-111 (2016) 1 – 6. doi:https://doi.org/10.1016/j.fusengdes.2016.03.067.

[13] F. Berger, K.-F.-L. Hau, Mass transfer in turbulent pipe flow measured by the electrochemical method, International Journal of Heat and Mass Transfer 20 (11) (1977) 1185 – 1194. doi:https://doi.org/10.1016/0017-9310(77)90127-2.

[14] X. Wang, Z. Dagan, L. Jiji, Heat transfer between a circular free impinging jet and a solid surface with non-uniform wall temperature or wall heat flux2. Solution for the boundary layer region, International Journal of Heat and Mass Transfer 32 (7) (1989) 1361 – 1371. doi:https://doi.org/10.1016/0017-9310(89)90035-5.

[15] H. C. Ji, R. Gardner, Numerical analysis of turbulent pipe flow in a transverse magnetic field, International Journal of Heat and Mass Transfer 40 (8) (1997) 1839 – 1851. doi:https://doi.org/10.1016/S0017-9310(96)00249-9.

[16] M. Al-Khawaja, R. Agarwal, R. Gardner, Numerical study of magneto-fluid-mechanic combined free-and-forced convection heat transfer, International Journal of Heat and Mass Transfer 42 (3) (1999) 467 – 475. doi:https://doi.org/10.1016/S0017-9310(98)00172-0.

[17] P. W. Humrickhouse, B. J. Merrill, Vacuum permeator analysis for extraction of tritium from DCLL blankets, Fusion Science and Technology 68 (2) (2015) 295–302. doi:https://doi.org/10.13182/FST14-941.

[18] S. Smolentsev, N. B. Morley, M. Abdou, Magnetohydrodynamic and thermal issues of the SiCf/SiC flow channel insert, Fusion Sci. Technol. 50 (1) (2006) 107–119. doi:https://doi.org/10.13182/FST06-A1226.

[19] F. R. Urgorri, S. Smolentsev, I. Fernández-Berceruelo, D. Rapisarda, I. Palermo, A. Ibarra, Magnetohydrodynamic and thermal analysis of PbLi flows in poloidal channels with flow channel insert for the EU-DCLL blanket, Nuclear Fusion 58 (10) (2018) 106001. doi:https://doi.org/10.1088/1741-4326/aad299.

[20] U. Müller, L. Bühler, Magnetohydrodynamics in channels and containers, Springer, 2001.

[21] P. Satyamurthy, P. Swain, V. Tiwari, I. Kirillov, D. Obukhov, D. Pertsev, Experiments and numerical MHD analysis of LLCB TBM test-section with NaK at 1T magnetic field, Fusion Engineering and Design 91 (2015) 44 – 51. doi:https://doi.org/10.1016/j.fusengdes.2014.12.015.

[22] S. Smolentsev, T. Rhodes, Y. Yan, A. Tassone, C. Mistrangelo, L. Bhler, F. R. Urgorri, Code-to-code comparison for a PbLi mixed-convection MHD flow, Fusion Science and Technology 76 (5) (2020) 653–669. doi:https://doi.org/10.1080/15361055.2020.1751378.

[23] D. Martelli, A. Venturini, M. Utili, Literature review of lead-lithium thermophysical properties, Fusion Engineering and Design 138 (2019) 183 – 195. doi:https://doi.org/10.1016/j.fusengdes.2018.11.028.

[24] P. W. Humrickhouse, P. Calderoni, B. J. Merrill, Implementation of tritium permeation models in the CFD code fluent, Fusion Science and Technology 60 (4) (2011) 1564–1567. doi:https://doi.org/10.13182/FST11-A12732.

[25] ANSYS Inc, ANSYS-Fluent UDF manual, release 15.0 Edition (November 2013).

[26] M. Baskes, A calculation of the surface recombination rate constant for hydrogen isotopes on metals, Journal of Nuclear Materials 92 (2) (1980) 318–324. doi:https://doi.org/10.1016/0022-3115(80)90117-8.

[27] F. R. Urgorri, C. Moreno, D. Rapisarda, Numerical investigation of the tritium permeation phenomenon through cooling plates in breeding blankets, Nuclear Fusion 61 (3) (2021) 036039. doi:https://doi.org/10.1088/1741-4326/abd194.

[28] O. Brice, B. Doyle, Steady state hydrogen transport in solids exposed to fusion reactor plasmas: Part I: Theory, Journal of Nuclear Materials 120 (2) (1984) 230–244. doi:https://doi.org/10.1016/0022-3115(84)90061-8.

[29] G. A. Esteban, A. Pea, I. Urra, F. Legarda, B. Riccardi, Hydrogen transport and trapping in EUROFER'97, J. Nucl. Mater. 367-370 (2007) 473–477.

[30] F. Reiter, Solubility and diffusivity of hydrogen isotopes in liquid Pb-17Li, Fusion Eng. Des. 14 (1997) 207–211.

[31] S. Smolentsev, N. Vetcha, M. Abdou, Effect of a magnetic field on stability and transitions in liquid breeder flows in a blanket, Fusion Engineering and Design 88 (6) (2013) 607–610. doi:https://doi.org/10.1016/j.fusengdes.2013.04.001.

[32] E. N. Sieder, G. E. Tate, Heat transfer and pressure drop of liquids in tubes, Industrial and Engineering Chemistry 28 (12) (1936) 1429–1435.

[33] P. Harriott, R. Hamilton, Solid-liquid mass transfer in turbulent

pipe flow, Chemical Engineering Science 20 (12) (1965) 1073 – 1078. doi:https://doi.org/10.1016/0009-2509(65)80110-5.

[34] W. H. Linton, T. K. Sherwood, Mass transfer from solid shapes to water in streamline and turbulent flow, Chemical Engineering Progress 46 (1950) 258.

[35] R. A. Gardner, Laminar pipe flow in a transverse magnetic field with heat transfer, International Journal of Heat and Mass Transfer 11 (6) (1968) 1076–1081. doi:https://doi.org/10.1016/0017-9310(68)90014-8.

[36] I. Fernández-Berceruelo, M. Gonzalez, I. Palermo, F. Urgorri, D. Rapisarda, Large-scale behavior of sandwich-like FCI components within the EU-DCLL operational conditions, Fusion Engineering and Design 136 (2018) 633–638. doi:https://doi.org/10.1016/j.fusengdes.2018.03.044.